Components of wall shear rate in wavy Taylor–Couette flow

Magdalena Kristiawan, Tomáš Jirout, Vaclav Sobolik

A8.

Experimental Thermal and Fluid Science 35 (2011) 1304–1312

Contents lists available at ScienceDirect

Experimental Thermal and Fluid Science

journal homepage: www.elsevier.com/locate/etfs

Components of wall shear rate in wavy Taylor–Couette flow

Magdalena Kristiawan [a,*], Tomáš Jirout [b], Václav Sobolík [a]

[a] University of La Rochelle, LEPTIAB, Avenue Michel Crépeau, 17042 La Rochelle, France
[b] Czech Technical University, Faculty of Mechanical Engineering, Technická 4, Prague, Czech Republic

ARTICLE INFO

Article history:
Received 5 December 2010
Received in revised form 25 March 2011
Accepted 23 April 2011
Available online 30 April 2011

Keywords:
Taylor–Couette
Azimuthal wave
Wall shear rate
Electrodiffusion method

ABSTRACT

The time-resolved axial and azimuthal components of the wall shear rate were measured as function of Reynolds number by a three-segment electrodiffusion probe flush mounted in the inner wall of the outer fixed cylinder. The geometry was characterized by a radius ratio of 0.8 and an aspect ratio of 44. The axial distribution of the wall shear rate components was obtained by sweeping the vortices along the probe using a slow axial flow. The wavelength and phase celerity of azimuthal waves, axial wavelength of vortices and their drifting velocity were calculated from the limiting diffusion currents measured by three simple electrodiffusion probes.

1. Introduction

The laminar flow in the gap between an inner rotating and outer fixed coaxial cylinders becomes unstable at critical Reynolds number due to centrifugal forces. Toroidal counter-rotating Taylor vortices with an axial wavelength equal approximately to the gap width replace original Couette flow [1]. The critical Reynolds number of the onset of Taylor vortices depends on the radius ratio of the cylinders [2,3]. This number does not depend on the aspect ratio Γ (wavelength versus width of the gap) with the exception of low values of Γ.

At higher rotation rates, the axisymmetric Taylor vortices become instable and azimuthal waves are superposed on them. The onset of azimuthal waves is strongly affected by end effects [4]. Even for an aspect ratio as great as 40, the onset of waves occurred at a Reynolds number greater than that at larger aspect ratios. Jones [5,6] calculated numerically the stability of Taylor vortices for radius ratios in the range $0.5 < \eta < 1$ using the approximation of infinite length cylinder.

Further increase in rotation rate induces azimuthal waves with modulated amplitude, then turbulent flow occurs in cells occupied earlier by vortices and, finally, the turbulent flow spreads throughout the whole gap.

Although the stability of supercritical circular Couette flow has been studied extensively, results for the velocity field of the flow are limited. Using finite-difference method, Fasel and Booz [7] calculated velocity fields of axisymmetric Taylor vortex flow in wide gap, $\eta = 0.5$, for the Reynolds number as high as $100Re_c$. Sengupta et al. [8] used Fluent for calculation of the velocity field of Taylor vortices in an narrower gap, $\eta = 0.8$, for a Reynolds number of 253. Marcus [9] simulated numerically non-axisymmetric wavy vortex flow in $\eta = 0.875$ and up to $15Re_c$.

Akonur and Lueptow [10] used particle image velocimetry for measurements of the azimuthal and radial velocities in latitudinal planes perpendicular to the axis of rotation of wavy Taylor–Couette flow characterized by a radius ratio of 0.81. These measurements were matched to measurements of the axial and radial velocity in several meridional planes with the aim to get time-resolved, three-dimensional, three-component velocity field for wavy Taylor–Couette flow. The results were published for three Reynolds numbers (124.3, 240.8 and 585.5). The PIV technique was also applied by Abcha et al. [11] for the measurements of the axial and radial velocity components of different instability modes in a geometry characterized by the radius ratio 0.8 and aspect ratio 45.9.

A vast number of applications of the Taylor–Couette flow (TCF) as reactor have been proposed, covering the field of catalytic [12], biocatalytic [13], electrochemical [14–16], photochemical [17] and polymerization reactions [18,19] as well as the mass transfer operations, such as counter current extraction [20], tangential filtration [21] and crystallization [22].

Many studies concerning flow patterns in TCF have been accomplished, but the knowledge of local wall shear rates in wavy and higher modes of TCF is only qualitative. This quantity is primordial for the applications like membrane filtration [23], the reactors with catalyst or immobilised enzyme [24] and the bioreactors

* Corresponding author. Tel.: +33 5 46 45 87 80; fax: +33 5 46 45 86 16.
E-mail address: magdanana@yahoo.com (M. Kristiawan).

0894-1777/$ - see front matter © 2011 Elsevier Inc. All rights reserved.
doi:10.1016/j.expthermflusci.2011.04.018

Nomenclature

A_z	amplitude of the axial component of wall shear rate averaged over one wave
a	maximum amplitude of azimuthal waves
d	width of gap between cylinders
d_e	probes diameter
D	coefficient of diffusion
f	frequency
h	height of vortex pair
I_1, I_2, I_3	limiting diffusion currents of three-segment probe
I_4, I_5, I_6	limiting diffusion currents of simple probes
I_{tot}	sum of currents I_1, I_2, I_3
K, b	coefficients in relation $I_{tot} = K\gamma^b$
L	length of gap between cylinders
l_{eq}	equivalent length of probe, $l_{eq} = 0.82d_e$
n	number of waves along the perimeter
Pe	Peclet number, $Pe = \gamma l_{eq}^2/D$
R_1, R_2	radius of the inner and outer cylinders
Re	Reynolds number, $Re = \Omega d R_1/\nu$
Re_{ax}	axial Reynolds number, $Re_{ax} = v_m d/\nu$
R_{44}	autocorrelation function of current 4
R_{45}	correlation of current 5 with respect to current 4
t_{d55}	time of the passage of vortex pair along probe 5
t_{d56}	time of the vortex passage from probes 5 to probe 6
t_{w44}	period of azimuthal waves
t_{w45}	time of wave passage between probes 4 and 5
t	time
ν	kinematic viscosity
v_d	drifting velocity of vortices
v_m	mean velocity of superposed axial flow
z	axial distance
x	critical region of an impinging jet

Greek letters

Γ	aspect ratio, $\Gamma = L/d$
γ	wall shear rate
η	radius ratios, $\eta = R_1/R_2$
Ω_w	angular velocity of azimuthal waves
Ω	angular velocity of the inner cylinder
τ	shear stress
δ	thickness of the concentration boundary layer

Index

c	transition from Couette flow to Taylor vortex flow
f	averaged over one azimuthal wave (perimeter)
θ	azimuthal
max	maximum
m	mean value over vortex height
min	minimum
r	radial
z	axial

containing shear sensitive cells [25]. The mean values of wall shear rate are known from the torque measurements [26,27] and linear theories [28]. However the wall shear rates of the wavy TCF are functions of space and time. Their fluctuations and especially their maxima are the most important quantity in the above mentioned applications. The experimental methods like Laser-Doppler anemometry [29,30] and PIV [10] do not allow measurements in the wall vicinity which are necessary for correct evaluation of wall shear rates.

The electrodiffusion diagnostics (ED) is a convenient nonintrusive method for measurements of wall shear rates [31]. Using three-segment micro-probes, the components of wall shear rate can be measured [32]. In this work, the axial and azimuthal components of the instantaneous shear rate on the wall of the outer fixed cylinder were measured as a function of rotation rate of the inner cylinder in the geometry characterized by radius ratio $\eta = 0.8$ and aspect ratio Γ about 43. The axial distribution of the wall shear rate components was obtained by sweeping wavy vortices along the fixed probes using a slow axial flow. The method of the vortex displacement by axial flow was already used by Townsend [33] for determining the velocity field of the toroidal vortices by the fixed hot wire anemometers. We also determined the number of azimuthal waves, their phase celerity, axial wavelength of vortices and their drifting velocity from the correlations of the limiting diffusion currents measured by an array of simple probes. This technique enabled us to obtain the mean azimuthal wall shear rate of a vortex pair with an arbitrary wavelength in contrast to the torque measurements which results in the wall shear rate averaged over the whole gap height. Moreover the torque measurements are distorted by the end effects, especially for low depth of liquid.

The electrodiffusion measurements of wall shear rate components for supercritical Couette flow carried out in this paper had several objectives. The first objective was to get detailed space–time cartography of wall shear rate components at several Reynolds numbers. This knowledge can be used for calculation of the instantaneous local wall shear stress via viscosity function. The second objective was to compare the wall shear rate components with the data on velocity fields published by Akonur and Lueptow [10]. The third objective was to verify the theory of inviscid cores surrounded by boundary layers proposed by Batchelor in the paper by Batchelor [26]. The last objective was to verify the numerical data of Jones [5,6] on the critical Reynolds number of the transition to wavy flow.

2. Experimental

The apparatus (see Fig. 1) consisted of an outer cylinder 3 made of a Plexiglas tube with an inner diameter of $R_2 = 62 \pm 0.1$ mm and an interchangeable inner Plexiglas cylinder 4. The inner cylinders had a length of 275 mm and diameter R_1 of 59 and 49.6 mm, respectively. The corresponding radius ratios, $\eta = R_1/R_2$, were 0.95 and 0.8. The larger cylinder was used for the calibration of electrodiffusion probe *in situ*. The inner cylinder was mounted on a stainless steal shaft 2 which had an upper ball bearing and bottom polyamide sliding bearing. The shaft was driven by a stepping motor with a step of 0.9° and a gear box with slow-down ratio 1:9. There was a plastic clutch between the shaft and gear box which also served as electrical insulation. The revolutions were controlled by a computer directly from the measuring software.

After filling the gap between the cylinders without rotation, the pump was stopped and the rotation rate corresponding to $Re = 80$ was adjusted. When laminar Couette flow was fully developed, Taylor vortices were established at Re equal to 100. Wavy vortex flow was then adjusted either by a sudden step or by increasing slowly the rotational rate (4 rpm/min) until determined Re.

The vortices were then swept by a slow axial flow. The liquid was alternatively pushed and pulled by a syringe with a volume of 100 mL at a rate of 0.0858 mL s^{-1} to an inlet tube in the bottom of the apparatus where it was distributed through four holes beneath the inner cylinder. The mean velocity of the axial flow in

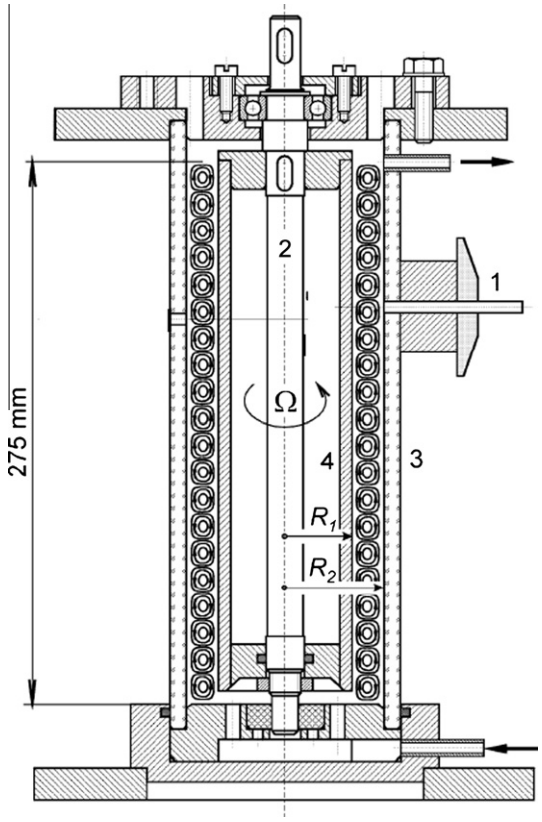

Fig. 1. Experimental set-up with Taylor vortices. 1 – Three-segment electrodiffusion probe, 2 – shaft, 3 – outer cylinder, 4 – inner cylinder.

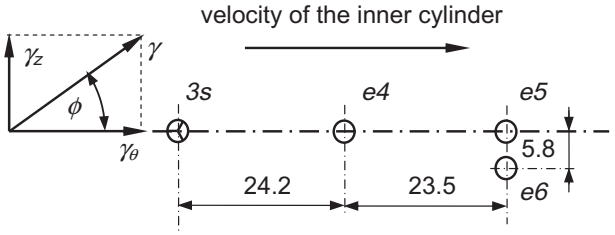

Fig. 2. Arrangement of electrodiffusion probes along the perimeter of the outer cylinder. The thick dash line stands for the cylinder perimeter. 3*s*: three-segment probe; *e*4, *e*5, *e*6: simple probes.

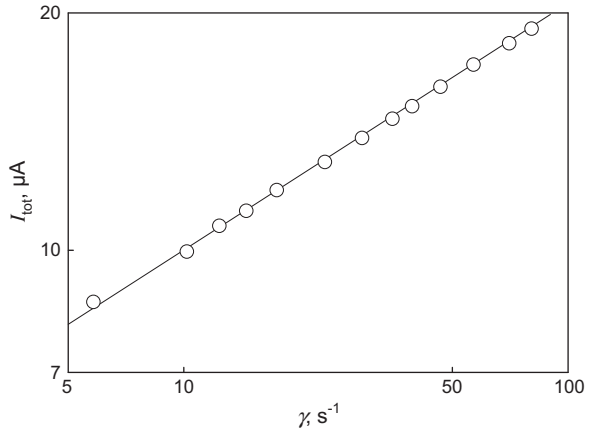

Fig. 3. Dependence of the total current of three-segment probe on wall shear rate. Solid line stands for $I_{tot} = 5.07\gamma^{0.31}$ for $\gamma \leqslant 80\ s^{-1}$.

the annular gap was 0.079 mm s^{-1} which corresponds to a wall shear rate of 0.074 s^{-1} and an axial Reynolds number of 0.49. As the axial flow direction was alternatively down and up and the free surface followed this motion, the aspect ratio varied between 40 and 44. At least one pair of vortices was swept up and down along the probes to verify that the flow structure is not deformed due to the axial motion. We did not observe any effect of this slow axial flow on the characteristics of vortices which is in accord with the numerical simulations of Recktenwald et al. [3]. They found that for an axial Reynolds number of 0.49, the critical Reynolds number increased by 0.009%. According to the linear stability analysis of Chung and Astill [34], there is practically no change in Re_c and axial wavelength of the vortices for $Re_{ax} = 0.49$.

A three-segment probe and three simple circular probes, all having the diameter d_e of 0.5 mm, were flush mounted in the inner wall of the outer fixed cylinder with zero overlapping. In this way, they did not disturb the flow. The electrodiffusion method is based on the measurement of the limiting diffusion current on the working electrode which depends on convective mass transfer at the electrode. As the concentration boundary layer is much thinner than the momentum boundary layer, it is assumed that the velocity profile in the concentration boundary layer is linear with a slope equal to the wall shear rate. The thickness of the concentration boundary layer δ depends on the wall shear rate γ, the coefficient of diffusion ($D = 7.8 \times 10^{-10}$ m^2/s) and the equivalent length of probe ($l_{eq} = 0.82 d_e$). The mean thickness can be estimated as $\delta = 1.238(Dl_{eq}/\gamma)^{1/3}$ [35]. In our case, the wall shear rate was measured in a layer of 49.5 μm and 14.5 μm for $\gamma = 5\ s^{-1}$ and 200 s^{-1}, respectively. The principle of electrodiffusion method and measurements of wall shear rate components using three-segment probe were described elsewhere [36]. The arrangement of the probes along the perimeter is shown in Fig. 2. The azimuthal γ_θ, and axial γ_z components of the wall shear rate γ were measured by the three-segment probe 3*s*. The data acquisitions were done by a six channels potentiostat and software developed under Turbo Pascal. The data were treated by a program written in the freeware Scilab.

For steady flow at high Peclet numbers $\left(Pe = \gamma l_{eq}^2/D\right)$ the Leveque relation holds between the limiting diffusion current and wall shear rate, $I_{tot} = K\gamma^{1/3}$. As our Peclet numbers were not high enough, the three-segment probe was calibrated in the small gap ($\eta = 0.95$) where the laminar Couette flow with wall shear rates in the interval (5; 80 s^{-1}) was adjusted. The sum of the segment currents was measured as a function of γ, see Fig. 3. The shear rates measured in our experiments ($\eta = 0.8$) were also superior to 80 s^{-1}. Using the results of numerical calculations of Geshev and Safarova [37], we divided the interval of the measured shear rates into two power law sections ($I_{tot} = K\gamma^b$), one for the shear rates inferior to 80 s^{-1} with corresponding $b = 0.31$ and the other section for the shear rates superior to 80 s^{-1} with $b = 0.325$. Typical values of K were evaluated from the calibration data as follows $K = 5.07$ for $b = 0.31$ and $K = 4.75$ for $b = 0.325$. The coefficients K and b were used for the calculation of wall shear rate magnitude from the sum of the measured currents in wavy flow. For the decomposition of wall shear rate into axial and azimuthal components, directional calibration at $\gamma = 20\ s^{-1}$ was curried up. The probe was turned by 15° steps and the currents of three segments were measured in the range (0°; 360°). The dependences of the segment currents normalized by the sum of the currents on the flow angle are called directional characteristics (see Fig. 4). Every flow angle corresponds to unique combination of three currents.

The above given method of the wall shear rate calculation from the measured limiting diffusion currents holds for steady and quasi-steady flows. If the flow is not steady, the inertia of diffusion boundary layer manifests itself as a filter which diminishes ampli-

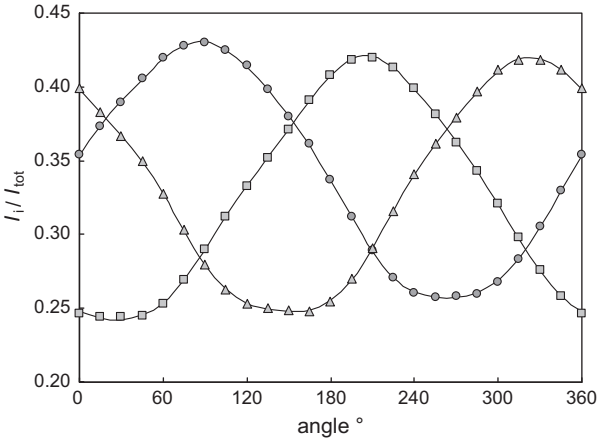

Fig. 4. Dependence of normalized segment currents on the angle of flow near the wall.

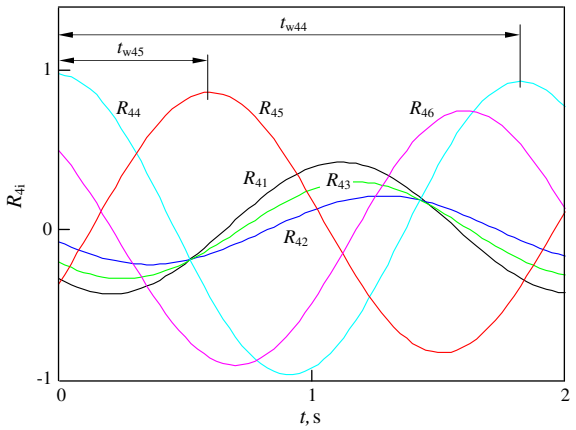

Fig. 6. Correlation of currents shown in Fig. 5 with respect to the current I_4.

tude and cause phase shift. The method of Sobolik et al. [38] was used for the calculation of absolute values of γ from the measured currents. Rehimi et al. [39] verified this method by numerical simulations. The inertia of the diffusion boundary layer has also an effect on the directional resolution of three-segment probes, but this problem has not been solved until yet. Therefore the flow angle was calculated under the assumption of quasi-steady flow.

The working solution was a 25 mol m^{-3} equimolar potassium ferri/ferrocyanide aqueous solution with 1.5 mass% K_2SO_4 as supporting electrolyte. A kinematic viscosity of 1.053×10^{-6} m^2 s^{-1} was measured by an Ubbelohde viscometer at 22 °C and a density of 1007 kg m^{-3} by a pycnometer. The behavior of the solution was purely Newtonien [40]. The measured critical Reynolds number of the onset of Taylor vortices (94.9) was in agreement with 94.8 referred by Ali et al. [41].

Different flow regimes were distinguished from the course of the limiting diffusion currents delivered by the three-segment probe. For a steady laminar flow, the currents ratio is constant. The axial flow component of Taylor vortices changes this currents ratio. The wavy vortex flow manifests itself by the current oscillations.

The limiting diffusion current histories measured by the three-segment probe (I_1, I_2, I_3) and three simple probes (I_4, I_5, I_6) in wavy vortex flow at $Re = 646$ are shown in Fig. 5. The measurements were taken over about one and half vortex pairs with a sampling frequency of 40 s^{-1}. The electric noise was removed by a low pass

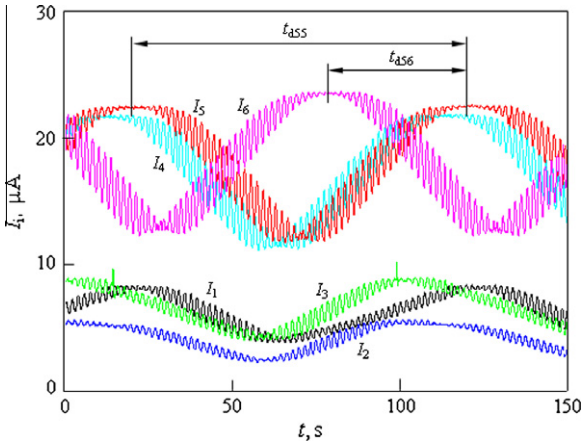

Fig. 5. Current history of three-segment probe (currents I_1, I_2 and I_3) and simple probes (currents I_4, I_5 and I_6) at $Re = 646$.

Butterworth filter of order 3 with a low pass frequency corresponding to 20 points. The signals have two periods. The azimuthal waves manifest themselves by the signal oscillations with the short period. The long period, t_{d55}, corresponds to the passage of vortex pairs along the probe. The drifting velocity of vortices was calculated from the time necessary for a vortex to cover the axial distance (5.8 mm) between the probes $e5$ and $e6$. This time corresponds to the lag t_{d56} of the currents I_5 and I_6. Vortex height was obtained by multiplication of the drifting velocity by the vortex period.

The period and celerity of azimuthal waves were calculated from the currents I_4 and I_5. For this aim the current correlations with respect to the current I_4 were calculated (see Fig. 6). The wave period equals to the period of the correlations. This period is denoted as t_{w44} on the autocorrelation function R_{44}. This period was also found on the spectral density function calculated by the fast Fourier transform. The celerity of azimuthal waves was calculated from the time lag of the currents delivered by $e4$ and $e5$ and the distance between these electrodes (23.5 mm). This time corresponds to the lag t_{w45} between the correlations R_{44} and R_{45}. The length of azimuthal waves was then calculated from their celerity and period. The number of azimuthal waves was obtained by division of the perimeter of the outer cylinder by the wave length. An entire number of waves was obtained with an accuracy of 3.5%. The axial wave length of vortices was obtained with a similar accuracy.

Experimental uncertainty in wall shear rate measurements, typically 6% in absolute value and 3° in flow angle exceeds other purely mechanical uncertainties such as tolerances of the cylinders, the error in the rotational rate or physical uncertainties such as accuracy of the time correlation. The error in wall shear rate measurements was due to activity variation (fouling) of the electrode surface. Typical variation of electrical current within 1.8% in the calibration before and after series of experiments results in $2^{1/b} = 6.28\%$ variation in the wall shear rate. Another uncertainty was in the irreproducibility of the flow pattern itself. Therefore triplicate measurements were carried out and the mean values were calculated. The electrodes were cleaned by a wet cloth and calibrated before each set of measurements.

3. Results and discussion

The absolute value and components of the wall shear rate measured at $Re = 646$ and calculated from the currents I_1, I_2, I_3 are shown in Fig. 7 as a function of time normalized by the time of vortex passage along the probe t_{d55}. As we have known the drifting velocity of vortices, the time was transformed into axial distance z ($z = tv_d$). The z-coordinate concerns the wavelength of vortices

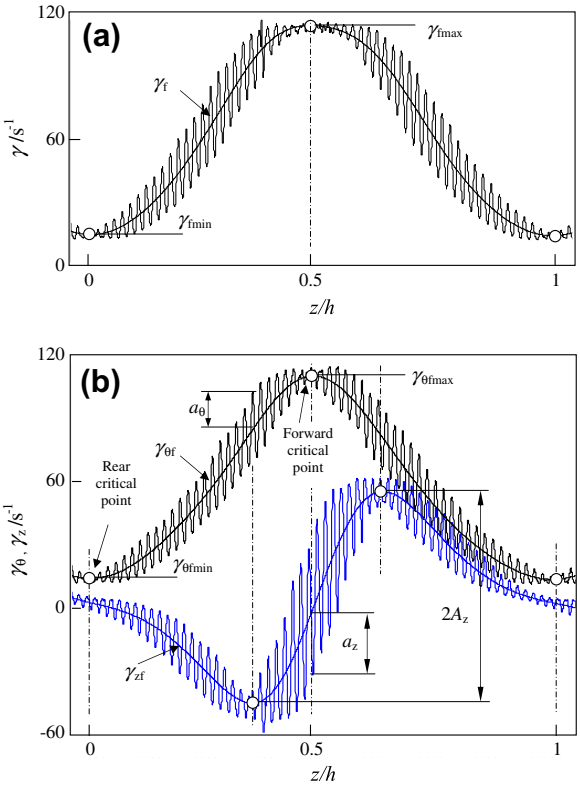

Fig. 7. Wall shear rate (a) and its components (b) measured at $Re = 646$ in three waves mode.

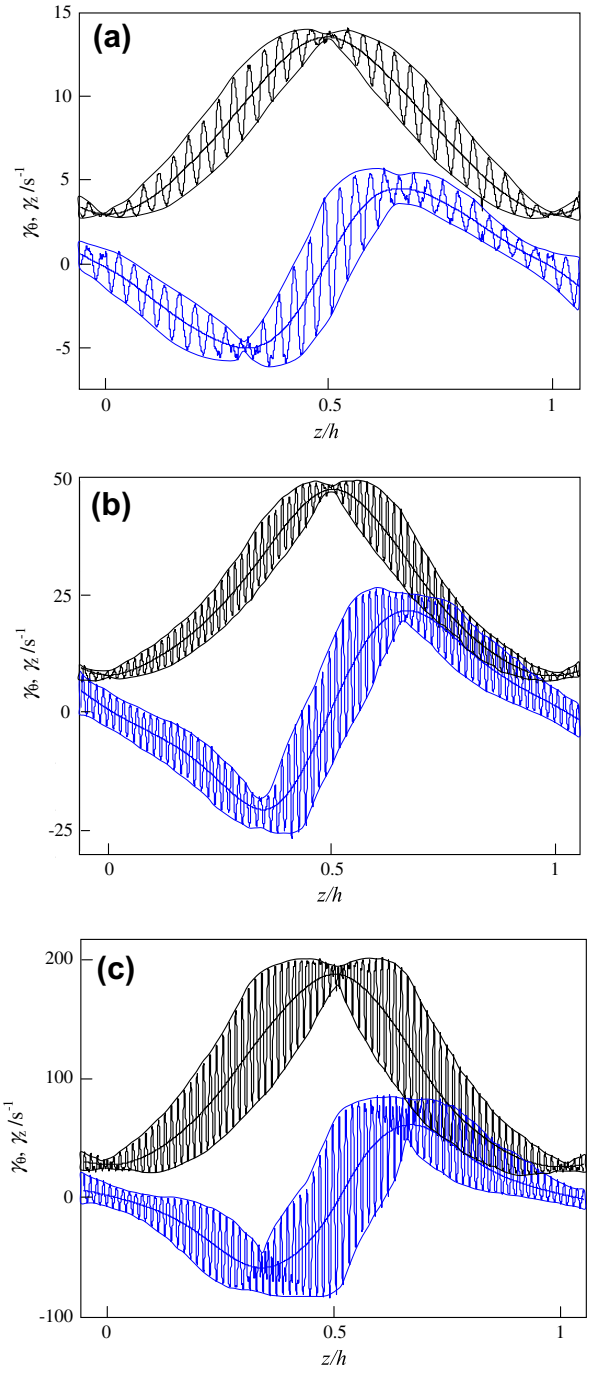

Fig. 8. Wall shear rate components measured at (a) $Re = 193$ in three waves mode, (b) $Re = 405$ in four waves mode, and (c) $Re = 967$ in two waves mode.

but it is irrelevant for the wavelength of azimuthal waves. The period of the oscillations in Fig. 7 is a function of the length and celerity of azimuthal waves and drifting velocity of vortices. This period increase with decreasing number and celerity of waves, and with decreasing drifting velocity of vortex.

Several notions for the description of wall shear rate and its components were introduced. The meaning of different symbols is apparent from Fig. 7. The vortices are described by functions γ_f, $\gamma_{\theta f}$ and γ_{zf}, which are the wall shear rate and their components averaged over azimuthal waves, or in another words averaged over perimeter. To obtain these functions the azimuthal waves were removed by a Butterworth filter of order 3 with a low pass frequency corresponding to 1000 points. The course of filtered wall shear rates and their components is similar to the wall shear rates in Taylor–Couette non-wavy flow [42]. The wall shear rate γ_f and azimuthal component $\gamma_{\theta f}$ exhibit the same minima and maxima ($\gamma_{f\min} = \gamma_{\theta f\min} = \gamma_{\min}$, $\gamma_{f\max} = \gamma_{\theta f\max} = \gamma_{\max}$). At these points the axial component γ_{zf} has practically negligible value. We can say that γ_{zf} is symmetric with respect to zero. Its amplitude is denoted as A_z.

From the point of view of the axial component of wall shear rate, there are critical points located at the outer cylinder at the extremes of $\gamma_{\theta f}$. The outflow manifests itself at the forward critical point ($z/h = 0.5$, $\gamma_{\theta f\max}$) and the inflow at the rear critical point ($z/h = 0$, $\gamma_{\theta f\min}$). The variation of γ_{zf} is very steep with inflexion in the forward critical point. The outflow has the form of a narrow jet with high radial and azimuthal velocities. The course of $\gamma_{\theta f}$ is symmetric with respect to the critical points. This fact was also confirmed by visual observation. Abcha et al. [11] have presented figures of the mean values of several flow quantities. However their shear rate (Fig. 8g in [11]) does not exhibit the above mention symmetry at the wall.

The wall shear rate of azimuthal waves has azimuthal and axial components. The amplitudes of these components, which are functions of the axial coordinate z, are given by the oscillation envelopes in Fig. 7. The amplitudes of the axial component have maximum a_z in the forward critical point and they are very small in the rear critical point. The amplitudes of the azimuthal component are almost zero in the critical points. They have maxima a_θ at the extremes of γ_{zf}.

Increasing the rotational rate very slowly (1 rpm/min), we observed the transition from the Taylor vortex flow into wavy vortex flow with two azimuthal waves at $Re = 121.6$. This value is close to the value calculated by Jones [5]. From his Fig. 3, we deducted for $\eta = 0.8$ values of Reynolds number 110, 115.2 and 129 for 1, 2 and 3 waves, respectively. Akonur and Lueptow [10] have found the transition to two waves mode at the Reynolds number 126 for η equal

to 0.81. Our measurements of wall shear rate started at the Reynolds number equal to 193 where three azimuthal waves were strong enough to support the axial translation without deformation. In the range of Reynolds number (242–810), it was possible to install three waves mode by a sudden increase of rotational rate to determined *Re* from the fully developed Taylor vortices (*Re* = 100). However four waves mode, which was adjusted by increasing of rotational rate slowly (4 rpm/min), was more stable. At the Reynolds number superior to 967 two wave mode was always achieved no matter how the rotational rate was established. Two waves mode at *Re* > 967 is in agreement with the numerical simulation of Jones [6].

The components of wall shear rates measured at different rotation rate are shown in Fig. 8. At the lowest rotational rate, *Re* = 193 (Fig. 8a), three azimuthal waves were stable. The amplitude of the azimuthal component of wall shear rate oscillations was almost zero at the critical points. The amplitude of the axial component exhibited maximum at the forward critical point ($z/h = 0.5$) and a small value at the rear critical point ($z/h = 0, 1$). Minima of the axial amplitude are located at the extremes of γ_{zf}. At these points, the azimuthal amplitude exhibited maxima. This scenario was the same for all rotational rates.

The amplitudes of the azimuthal waves of successive vortices were not always the same. Slight differences of magnitude comparable with the accuracy of electrodiffusion measurements are manifested by the dissymmetry on each side of the forward critical point in Fig. 8b and c.

The axial component of the wall shear rate can be compared to the wall shear rate in classical impinging jet even if the azimuthal component in the forward critical point of wavy Taylor–Couette flow exhibits a maximum. According to the boundary layer theory [43], it holds for the critical region of an impinging jet that the wall shear rate is proportional to the distance from the critical point *x*. The maximum of the wall shear rate is at the transition from the critical zone to the wall jet region. The distribution of the wall shear rate fluctuations in function of *x* depends on the jet Reynolds number and the distance of the orifice from the plate [44]. Jones [6] concluded that the strong azimuthal jets at the outflow zone destabilize the flow making the vortices wavy. Coughlin and Marcus [45] supposed that the both radial and azimuthal jets and axial gradient of the azimuthal velocity are responsible for the waviness. Our results (Figs. 7 and 8) confirm these features. A strong azimuthal jet manifests itself by the maxima of $\gamma_{\theta f}$ and steep, linear variation of γ_{zf} in the outflow. The radial velocity of the jet can be deduced from the axial gradient of γ_{zf}, which increases with the increasing Reynolds number.

The character of the flow was verified by frequency spectra, see Fig. 9a and b. The first peak in Fig. 9b corresponds to a frequency $f_1 = 0.623$ Hz. This frequency is equal to the rotation rate 1.17 Hz multiplied by the dimensionless frequency of wave train 0.266 and the number of waves 2. The second (1.246 Hz) and third peak (1.86) are the harmonics of the base frequency. No other significant frequencies appeared which would correspond to modulation of the azimuthal waves.

Taylor–Couette flow was often studied by the torque measurements. As the torque can be deduced from the mean azimuthal wall shear rate, we had plotted $\gamma_{\theta m}$ in Fig. 10 as a function of the Reynolds number. The triangles correspond to the Taylor vortices [42] and the circles to the wavy vortices (gray to four waves, open to three waves and full to two waves). The dash and dot line corresponds to the hypothetical laminar Couette flow and the dotted line to the Taylor flow. The full line, which represents the best fit of the wavy vortices, has the equation $\gamma_{\theta m} = 0.003Re^{1.5}$. This exponent was also found by Batchelor [26] who supposed that the flow is steady and consists of inviscid cores surrounded by boundary layers. However, the theory of Batchelor does not give the value

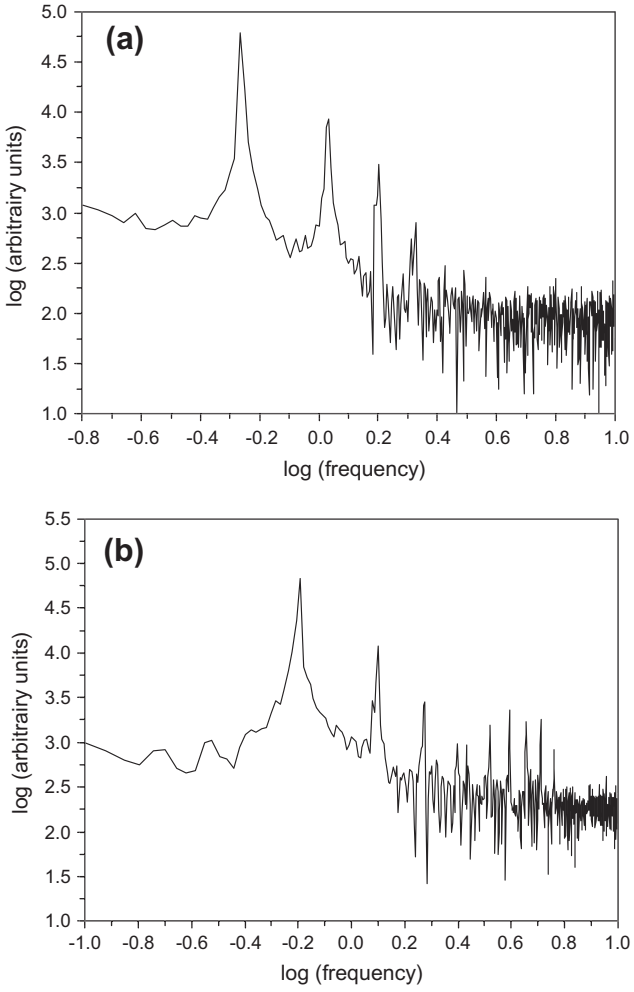

Fig. 9. Frequency spectra pour two waves mode. (a) Re = 967, 1st peak 0.54 Hz, 2nd peak 1.08 Hz, 3rd peak 1.62 Hz. (b) Re = 1130, 1st peak 0.623 Hz, 2nd peak 1.246 Hz, 3rd peak 1.86 Hz.

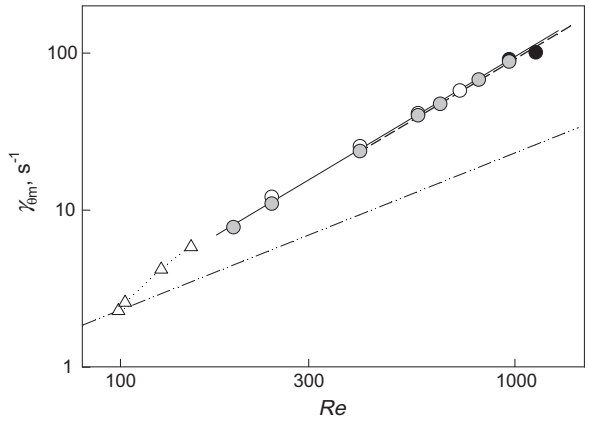

Fig. 10. Mean azimuthal wall shear rate as a function of Reynolds number. △ Taylor vortices [42], ○ wavy flow $n = 4$, ◍ wavy flow $n = 3$, ● wavy flow $n = 2$, — best fit of data $\gamma_{\theta m} = 0.003Re^{1.5}$, –·–· hypothetical laminar Couette flow, ··· best fit of Taylor vortices, – – – data by Wendt [27] $\gamma_{\theta m} = 0.00289Re^{1.5}$.

of the multiplication constant. Wendt [27] measured the torque in three geometries, $\eta = 0.68$, 0.85 and 0.935 with an uncertainty 3%. His results were interpolated for $\eta = 0.8$ to give $\gamma_{\theta m} = 0.00289Re^{1.5}$ in the interval $400 < \mathrm{Re} < 10^4$, see Lathrop et al. [46]. The accord with our measurements is within 3.5%

Table 1
Comparison of normalized mean azimuthal wall shear rate with normalized mean wall shear stress [10].

Akonur and Lueptow [10]			This work		
Re	$\tau_{r\theta}/\tau_{r\theta c}$	*n*	*Re*	$\gamma_{\theta m}/\gamma_{\theta c}$	*n*
241	4.5	4	242	5.1	3
590	15	4	568	17.2	4

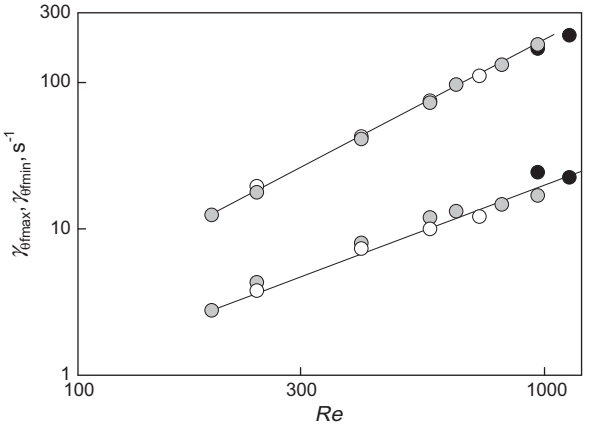

Fig. 11. Maximum and minimum of azimuthal wall shear rate as a function of Reynolds number. ○ wavy flow $n = 4$, ◍ wavy flow $n = 3$, ● wavy flow $n = 2$. –, best fit of data for $n = 3$ $\gamma_{\theta max} = 0.0019Re^{1.67}$.and $\gamma_{\theta min} = 0.005Re^{1.2}$.

Akonur and Lueptow [10] estimated the mean value of the azimuthal shear stress from the PIV measurements. These values were normalized by the shear stress at the transition to Taylor vortex flow, $\tau_{r\theta}/\tau_{r\theta c}$. As the shear stress is a linear function of the shear rate with viscosity as the multiplication constant, we can calculate this ratio from our measurements, see Table 1. Our values $\gamma_{\theta m}/\gamma_{\theta c}$ are about 15% higher at Reynolds number about 570. This deviation can be caused by the irreproducibility of the flow regimes, the accuracy of the electrodiffusion method and also by the inability of PIV to measure close enough to a wall. The last hypothesis is supported by the fact that the data on the shear stress [10] exhibit a discontinuity close to the wall.

For the prevention of membrane fouling the variations of wall shear stress are more important than mean values. Akonur and Lueptow [10] have found that for a Reynolds number of 585.5, the shear at the outer cylinder for the outflow boundary is more than three times higher than that for an inflow boundary. We have found this ratio ($\gamma_{\theta f max}/\gamma_{\theta f min}$) higher than six for a similar $Re = 568$. The discrepancies between the both methods can be explained by the fact that the electrodiffusion method measures in a thinner layer close to the wall than PIV technique. The particles used in the PIV had a diameter 14 μm whereas the thickness of the diffusion boundary layer, where we measured the shear rate, was about 25 μm at $Re = 568$. Bouabdallah [47] applied the electrodiffusion method for the measurements of wall shear rates in Taylor–Couette flow with $\eta = 0.82$, 0.909 and 0.954. We can compare our results on $\gamma_{\theta f max}$ and $\gamma_{\theta f min}$ with that of Bouabdallah [47] for $\eta = 0.909$. In both cases, the minimum values of shear rate approach the extrapolated values of laminar Couette flow. For *Re* equal to 200 and 1000 the ratios of maximum and minimum values are 1.6 and 2.2 [47], respectively, and 4.6 and 9.8 (our results), respectively. Lathrop et al. [46] used hot film anemometry for wall shear rate measurements but their results are presented as time series only.

The knowledge of maximum values of wall shear stress is important for the solicitation of microorganisms and prevention of membrane fouling. The values of $\gamma_{\theta f max}$ for three waves grew with Reynolds number with an exponent of 1.67, see Fig. 11. Practically, the data for all three numbers of azimuthal waves can be fitted by the same function.

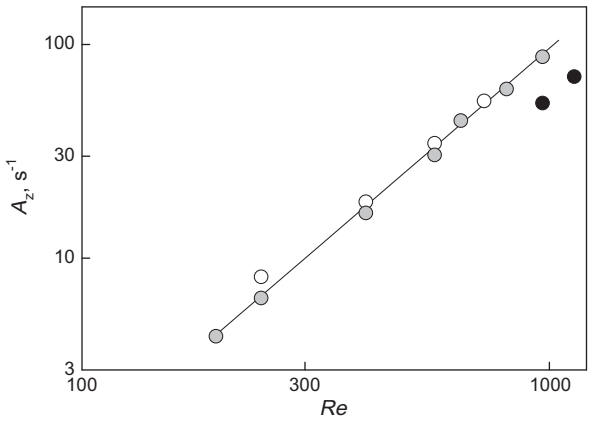

Fig. 12. Amplitude of the axial component of mean wall shear rate as a function of Reynolds number. For symbols see Fig. 11. — best fit of data for $n = 3$ $A_z = 0.00022Re^{1.88}$.

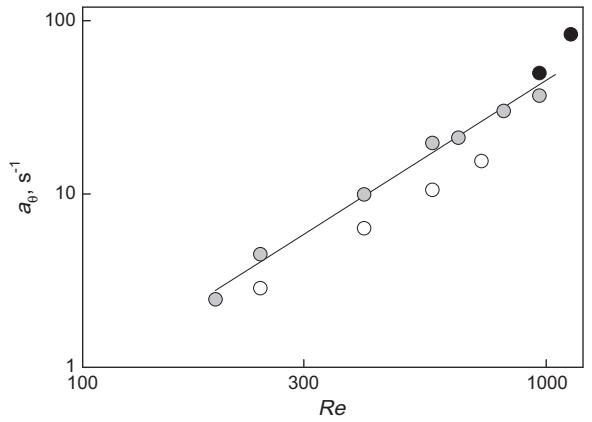

Fig. 13. Maximum of azimuthal amplitude of azimuthal waves as a function of Reynolds number. For symbols see Fig. 11. — best fit of data for $n = 3$, $a_\theta = 0.00036Re^{1.7}$.

The amplitude A_z of the axial component of averaged wall shear rate γ_{zf} grows with an exponent of 1.88, see Fig. 12, that is more rapidly than $\gamma_{\theta f max}$. However the values of A_z are lower than that of $\gamma_{\theta f max}$, especially for two azimuthal waves.

The maximum azimuthal amplitude a_θ of azimuthal waves depends on the number of waves, see Fig. 13. The amplitude grows up with increasing Reynolds number and with decreasing number of waves.

The maximum axial amplitude a_z also depends on the number of waves, see Fig. 14. The axial amplitude grows more rapidly with Reynolds number than the azimuthal amplitude.

It holds for all *Re*, that a_z is superior to a_θ. The maximum amplitude a_z is located in the forward critical point. However, the oscillation of the absolute value of the wall shear rate are almost negligible in this point, because a_θ is zero and $\gamma_{\theta f}$ has its maximum which is several times higher than a_z. A single electrode gives only scares information about fluctuations. It exhibits small oscillations in the forward critical point (outflow), see currents I_4, I_5 and I_6, in Fig. 5. One of the currents of the three-segment probe exhibits always fluctuations which manifest in the axial oscillations in the forward critical point.

The angular velocity of azimuthal waves normalized by the velocity of the inner cylinder is shown in Fig. 15. The exponential

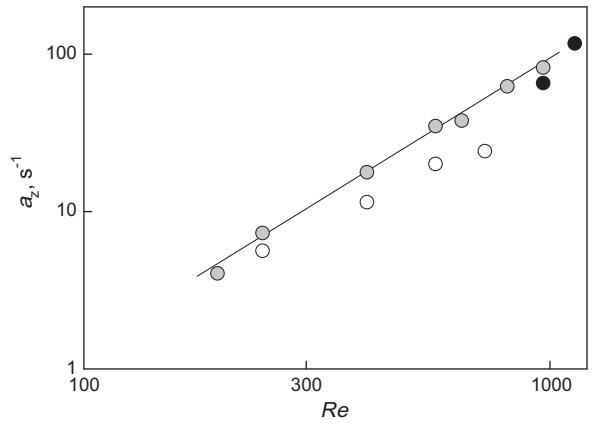

Fig. 14. Maximum of axial amplitude of azimuthal waves as a function of Reynolds number. For symbols see Fig. 11. — best fit of data for $n = 3$, $a_z = 0.0003Re^{1.83}$.

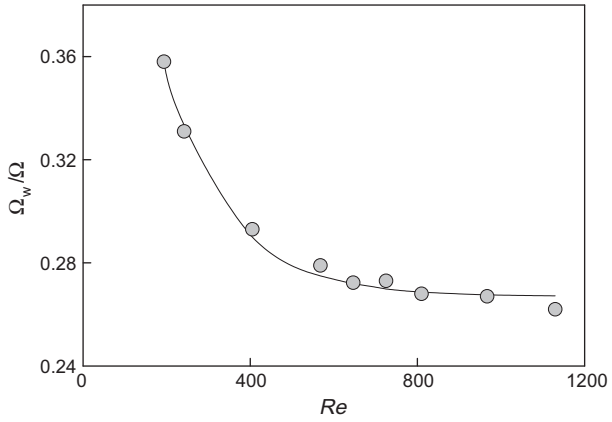

Fig. 15. Angular velocity of azimuthal waves normalized by the velocity of the inner cylinder for $n = 3$. — best fit of data $\Omega_w/\Omega = 0.267 + 0.32\exp(-Re/154)$.

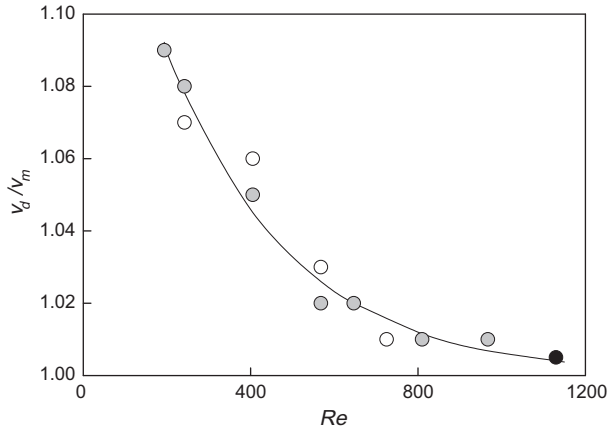

Fig. 16. Drifting velocity of vortices normalized by mean axial velocity. For symbols see Fig. 11. — best fit of data for $n = 3$, $v_d/v_m = 1 + 0.177\exp(-Re/295.3)$.

dependence on Reynolds number has an asymptote equal to 0.267. This value is in agreement with the numerical simulation of King et al. [48].

At the lowest *Re*, the drifting velocity of vortices was about 9% higher than the mean velocity of the axial flow, see Fig. 16. The drifting velocity decreased exponentially with increasing *Re* to a value of the mean velocity of the axial flow. Using perturbation theory, Snyder [49] predicted $v_d/v_m = 1.21$ for $\eta = 0.95$ at the transition from Couette flow to Taylor vortices. His experimental values diminished with increasing Reynolds number which is in accord with our measurements. Wereley and Lueptow [50] obtained a value of 1.17 for $\eta = 0.83$ by interpolation of the theoretical results of Recktenwald et al. [3]. Their experimental values lay below the theoretical.

The axial wavelength of vortices was in almost all cases lower than the double of the angular space ($h = 11$–12 mm, $2d = 12.4$ mm). Only at the highest Reynolds numbers (967 and 1130) the wavelength of vortices was superior (13.1 mm) to $2d$.

The course of azimuthal component averaged over perimeter is symmetric with respect to the critical points which is in concordance with the results of Akonur and Lueptow [10]. Her form is similar to the distribution in axisymmetric Taylor vortices [42]. However, the maximal values are more important in wavy flow. This similarity was also confirmed by Wang et al. [51] who compared the mean values of velocity components measured in wavy flow using PIV with the results of numerical simulations at the same Reynolds number supposing that the flow is axisymmetric.

4. Conclusions

Previous studies of Taylor–Couette wavy flow have never given components of time dependent wall shear rate. We have used three-segment electrodiffusion probe to measure these components in a large range of Reynolds numbers. The knowledge of the azimuthal and axial components of wall shear rate gives us an idea about the variations of the wall shear stress and flow direction in the wall vicinity. These variations are crucial for the prevention of membrane fouling and solicitation of microorganisms fixed at the wall.

The maximum values of wall shear rate are in forward critical point (outflow). They are equal to the azimuthal component as the axial component is zero at this point. The fluctuations of the azimuthal component are zero whereas the fluctuation of axial component achieved a maximum at this point. The oscillations have a similar character also in the rear critical point, where the wall shear rate and azimuthal component have a minimum and the axial component is near to zero.

The axial distributions of the wall shear rate components averaged over perimeter are similar to the distribution in steady Taylor vortices.

The space averaged wall shear rate, the maximum of azimuthal component, and the amplitudes of wall shear rate components increase with Reynolds number on the power between 1.5 and 1.9.

The wave celerity normalized by the velocity of the inner cylinder decreases exponentially with increasing rotational rate. The drifting velocity of vortices decreases with increasing Reynolds number.

The dependence of the mean azimuthal component of the wall shear rate on the angular velocity of the inner cylinder is in agreement with the theory of inviscid cores surrounded by boundary layers proposed by Batchelor [26]. The wall shear rate components exhibited the same features as described by Akonur and Lueptow [10].

Acknowledgments

This work was supported by the "Agence National de la Recherche", France, by the Grant Number ANR-08-BLAN-0184-01. The authors are indebted to referees for their pertinent comments.

References

[1] D. Coles, Transition in circular Couette flow, J. Fluid Mech. 21 (1965) 385–425.
[2] P.H. Roberts, The solution of the characteristic value problems, Appendix to R.J. Donnelly, K.W. Schwartz, experiments on the stability of viscous flow between rotating cylinders. VI. Finite-amplitude experiments, Proc. Roy. Soc. London A 283 (1965) 550–556.

[3] A. Recktenwald, .M. Lücke, H.W. Müller, Taylor vortex formation in axial through-flow: linear and weakly nonlinear analysis, Phys. Rev. E 48 (1993) 4444–4454.
[4] J.A. Cole, Taylor-vortex instability and annulus-length effects, J. Fluid Mech. 75 (1976) 1–15.
[5] C.A. Jones, Nonlinear Taylor vortices and their stability, J. Fluid Mech. 102 (1981) 249–261.
[6] C.A. Jones, The transition to wavy Taylor vortices, J. Fluid Mech. 157 (1985) 135–162.
[7] H. Fasel, O. Booz, Numerical investigation of supercritical Taylor-vortex flow for a wide gap, J. Fluid Mech. 138 (1984) 21–52.
[8] T.K. Sengupta, M.F. Kabir, A.K. Ray, A Taylor photocatalytic reactor for water purification, Ind. Eng. Chem. Res. 40 (2001) 5268.
[9] P.S. Marcus, Simulation of Taylor–Couette flow. Part 2. Numerical results for wavy-vortex flow with one travelling wave, J. Fluid Mech. 146 (1984) 65–113.
[10] A. Akonur, R.M. Lueptow, Three-dimensional velocity field for wavy Taylor–Couette flow, Phys. Fluids 15 (2003) 947–960.
[11] N. Abcha, N. Latrache, F. Dumouchel, I. Mutabazi, Qualitative relation between reflected light intensity, Exp. Fluids 45 (2008) 85–94.
[12] S. Cohen, D.M. Maron, Analysis of a rotating annular reactor in the vortex flow regime, Chem. Eng. Sci. 46 (1991) 123–134.
[13] G.V. Baron, P. Van Capellen, A novel bioreactor for immobilised cell systems, in: J.A.M. de Bont, J. Visser, B. Mattiasson, J. Tramper (Eds.), Physiology of Immobilized Cells, Elsevier, Amsterdam, 1990.
[14] T. Mizushina, The electrochemical method in transport phenomena, in: T.F. Irvine, J.P. Hartnett (Eds.), Advances in Heat Transfer, vol. 7, Academic Press, New York, 1971, pp. 87–161.
[15] Z.H. Gu, T.Z. Fahidy, Mass transport in the Taylor-vortex regime of rotating flow, Chem. Eng. Sci. 40 (1985) 1145–1153.
[16] F. Coeuret, J. Legrand, Mass transfer at the electrodes of concentric cylindrical reactors combining axial flow and rotation of the inner cylinder, Electrochim. Acta 26 (1981) 865–872.
[17] D. Haim, L.M. Pismen, Performance of a photo-chemical reactor in the regime of Taylor–Goertler vortical flow, Chem. Eng. Sci. 49 (1994) 1119–1129.
[18] V. Sinevic, R. Kuboi, A.W. Nienow, Power numbers, Taylor numbers and Taylor vortices in viscous Newtonian and non-Newtonian fluids, Chem. Eng. Sci. 41 (1986) 2915–2923.
[19] K. Kataoka, M. Okubo, Emulsion polymerization of styrene in a continuous Taylor vortex flow reactor, Chem. Eng. Sci. 50 (1995) 1409–1416.
[20] R.A. Leonard, G.J. Bernstein, R.H. Pelto, A.A. Ziegler, Liquid–liquid dispersion in turbulent Couette flow, AIChE J. 27 (1981) 495–503.
[21] U.B. Holechovsky, C.L. Cooney, Quantitative description of ultrafiltration in a rotating filtration device, AIChE J. 37 (1991) 1219–1227.
[22] S.H. Kang, S.G. Lee, W.M. Jung, M.C. Kim, W.S. Kim, C.K. Choi, R.S. Feigelson, Effect of Taylor vortices on calcium carbonate crystallization by gas–liquid reaction, J. Cryst. Growth 254 (2003) 196–205.
[23] C.K. Choi, J.Y. Park, W.C. Park, J.J. Kim, A study on dynamic separation of silica slurry using a rotating membrane filter: 2. Modelling of cake formation, J. Membr. Sci. 157 (1999) 177–187.
[24] P.K. Dutta, A.K. Ray, Experimental investigation of Taylor vortex photocatalytic reactor for water purification, Chem. Eng. Sci. 59 (2004) 5249–5259.
[25] S.J. Curran, A. Richard, R.A. Black, Quantitative experimental study of shear stresses and mixing in progressive flow regimes within annular-flow bioreactors, Chem. Eng. Sci. 59 (2004) 5859–5868.
[26] G.K. Batchelor, A theoretical model of the flow at speeds far above the critical. Appendix to R.J. Donnelly, N.J. Simon, an empirical torque relation for supercritical flow between rotating cylinders, J. Fluid Mech. 7 (1960) 401–418.
[27] F. Wendt, Turbulente Strömungen zwischen zwei rotierenden koaxialen Zylindern, Ing. Arch. 4 (1933) 577–595.
[28] P.M. Eagles, On the torque of wavy vortices, J. Fluid Mech. 62 (1974) 1–9.
[29] O. Fehrenbacher, R.C. Aldrege, J.T. Morgan, Turbulence structure in a Taylor–Couette apparatus, Exp. Therm. Fluid Sci. 32 (2007) 220–230.
[30] V. Vaezi, E.S. Oh, R.C. Aldredge, High-intensity turbulence measurements in a Taylor–Couette flow reactor, Exp. Therm. Fluid Sci. 15 (1997) 424–431.
[31] T.J. Hanratty, J.A. Campbell, Measurement of wall shear stress, in: R.J. Goldstein (Ed.), Fluid Mechanics Measurements, Hemisphere Publishing Corporation, Washington, 1983, pp. 519–615.
[32] O. Wein, V. Sobolik, Theory of direction sensitive probes for electrodiffusion measurement of wall velocity gradients, Collect. Czech. Chem. Commun. 52 (1987) 2169–2180.
[33] A.A. Townsend, Axisymmetric Coutte flow at large Taylor numbers, J. Fluid Mech. 144 (1984) 329–362.
[34] K.C. Chung, K.N. Astill, Hydrodynamic instability of viscous flow between rotating coaxial cylinders with fully developed axial flow, J. Fluid Mech. 81 (1977) 641–655.
[35] N.A. Pokryvaylo, O. Wein, N.D. Kovalevskaya, Electrodiffusion Diagnostics of Flows in Suspensions and Polymer Solutions, Nauka i Tekhnika, Minsk, 1988 (in Russian).
[36] V. Sobolik, Electrochemical study of Taylor–Couette flow by limiting diffusion current method, Collect. Czech. Chem. Commun. 64 (1999) 1193–1210.
[37] P.I. Geshev, N.S. Safarova, Angular and transient characteristics of circular electrochemical friction probes, Int. J. Heat Mass Transfer 42 (1999) 3138–3188.
[38] V. Sobolik, O. Wein, J. Cermak, Simultaneous measurement of film thickness and wall shear stress in wavy-film flow of non-Newtonian fluids, Collect. Czech. Chem. Commun. 52 (1987) 913–928.
[39] F. Rehimi, F. Aloui, S. Ben Nasrallah, L. Doubliez, J. Legrand, Inverse method for electrodiffusion diagnostics of flows, Int. J. Heat Mass Transfer 49 (2006) 1242–1254.
[40] M. Abdulagatov, N.D. Azizov, Thermal conductivity and viscosity of aqueous K_2SO_4 solutions at temperatures from 298 to 575 K and at pressures up to 30 MPa, Int. J. Thermophys. 26 (2005) 593–635.
[41] M.E. Ali, D. Mitra, J.A. Schwille, R.M. Lueptow, Hydrodynamic stability of a suspension in cylindrical Couette flow, Phys. Fluids 14 (2002) 1236–1243.
[42] V. Sobolik, T. Jirout, J. Havlica, M. Kristiawan, Wall shear rates in Taylor vortex flow, J. Appl. Fluid Mech. 4 (2011).
[43] H. Schlichting, K. Gersten, Boundary Layer Theory, 8th revisited and enlarged ed., Springer, Berlin, 2003. p. 118.
[44] S.V. Alekseenko, D.M. Markovich, Electrodiffusion diagnostics of wall shear stresses in impinging jets, J. Appl. Electrochem. 24 (1994) 626–631.
[45] K.T. Coughlin, P.S. Marcus, Modulated waves in Taylor–Couette flow: part 2. Numerical simulation, J. Fluid Mech. 234 (1992) 19–46.
[46] D.P. Lathrop, J. Fineberg, H.L. Swinney, Transition to shear-driven turbulence in Couette–Taylor flow, Phys. Rev. A 46 (1992) 6390–6405.
[47] A. Bouabdallah, Effect of the geometric factor on the laminar-turbulent transition in Taylor–Couette flow, in: N. Boccara (Ed.), Symmetries and Broken Symmetries in Condensed Matter Physics, IDSET, Paris, France, 1981, pp. 407–417.
[48] G.P. King, Y.L. Lee, H.L. Swinney, P.S. Marcus, Wave speeds in wavy Taylor-vortex flow, J. Fluid Mech. 141 (1984) 365–390.
[49] H.A. Snyder, Experiments on the stability of spiral flow at low axial Reynolds numbers, Proc. Roy. Soc. London, Ser. A 265 (1962) 198–214.
[50] S.T. Wereley, R.M. Lueptow, Velocity field for Taylor–Couette flow with an axial flow, Phys. Fluids 11 (1999) 2637–3649.
[51] L. Wang, D.L. Marchisio, R.D. Vigil, R.O. Fox, CFD simulation of aggregation and breakage processes in laminar Taylor–Couette flow, J. Colloid Interf. Sci. 282 (2005) 380–396.